Research Square

Preprints are preliminary reports that have not undergone peer review.
They should not be considered conclusive, used to inform clinical practice,
or referenced by the media as validated information.

Effect of Calcination Temperature on the Synthesis of Silicon Carbide from Rice Husk with Copper Additive

Do Trung Kien Kieu

kieudotrungkien@hcmut.edu.vn

Ho Chi Minh City University of Technology (HCMUT)

Ngoc Minh Huynh

Ho Chi Minh City University of Technology (HCMUT)

Vu Uyen Nhi Nguyen

Ho Chi Minh City University of Technology (HCMUT)

Le My Duyen Tran

Ho Chi Minh City University of Technology (HCMUT)

Article

Keywords:

Posted Date: June 24th, 2026

DOI: https://doi.org/10.21203/rs.3.rs-10006951/v1

License: This work is licensed under a Creative Commons Attribution 4.0 International License.
Read Full License

Additional Declarations: No competing interests reported.

Effect of Calcination Temperature on the Synthesis of Silicon Carbide from Rice Husk with Copper Additive

Kieu Do Trung Kien[1,2*], Huynh Ngoc Minh[1,2], Nguyen Vu Uyen Nhi[1,2], Tran Le My Duyen[1,2]

[1] Faculty of Materials Technology, Ho Chi Minh City University of Technology (HCMUT), 268 Ly Thuong Kiet Street, Dien Hong Ward, Ho Chi Minh City, Vietnam.

[2] Vietnam National University Ho Chi Minh City, Linh Trung Ward, Ho Chi Minh City, Vietnam.

[*]Corresponding author: kieudotrungkien@hcmut.edu.vn

Abstract

The synthesis of silicon carbide from rice husk typically requires temperatures above 1500 °C due to limitations in solid-state diffusion. In this study, a Cu-catalyzed carbothermal reduction route was investigated using a rice husk–silica gel mixture at a fixed mass ratio of 1:1.4 over the temperature range of 900–1300 °C. After HF purification, a high SiC content of 88.47% (ISO 21068-2:2008) was achieved at 1300 °C, which is approximately twice that obtained by non-catalytic pyrolysis (40–60% at 1600 °C). Three distinct kinetic regimes were identified: 900–1100 °C, characterized by a gradual increase in SiC yield (4.63% per 100 °C); 1100–1200 °C, showing a sharp increase (8.48% per 100 °C after purification); and 1200–1300 °C, where the reaction approached saturation. The presence of Cu promotes a Vapor–Liquid–Solid mechanism via the formation of a low-temperature Si–Cu eutectic (~800 °C), thereby significantly enhancing atomic diffusion between the liquid and solid phases. XRD analysis confirmed the formation of 3C- and 4H-SiC polytypes, while FTIR spectra revealed characteristic Si–C vibration bands at 809 and 624 cm^{-1}. HF treatment effectively removed residual SiO_2 and Cu oxides, as evidenced by SEM/EDX analysis. The combined catalytic assistance and selective post-purification enable high-purity SiC formation at significantly reduced temperatures, demonstrating an efficient pathway for converting biomass-derived precursors into advanced ceramic materials.

1. Introduction

Silicon carbide (SiC) is a strategic material with widespread applications in abrasives, advanced structural ceramics, high-temperature components, power electronics, and lithium-ion batteries, owing to its exceptional hardness, high thermal conductivity, and outstanding thermal stability in vacuum environments.[1-4] Industrial-scale SiC production is dominated by the Acheson process ($SiO_2 + 3C \rightarrow SiC + 2CO$), which requires extremely high temperatures of 2200–2500 °C in electric arc furnaces, resulting in high energy consumption (11.6 MWh t^{-1} SiC) and substantial CO_2 emissions (9.2 t CO_2 t^{-1} product).[5-7] Driven by the rapid growth of electric vehicles and renewable energy systems, the global SiC market reached approximately USD 3.5 billion in 2024, with an annual growth rate of about 25%. However, 60–70% of high-purity crystalline SiC remains dependent on production in China, mainly due to the high manufacturing costs associated with energy-intensive processes in developed countries. Consequently, the environmental and economic limitations of the Acheson process have motivated increasing interest in green chemistry strategies that replace synthetic silica and fossil-derived carbon with sustainable biomass resources.[8-10]

Vietnam, the world's third-largest rice exporter (8.1 million tons in 2025), generates approximately 18–20 million tons of rice husk annually, corresponding to 3.6–4.0 million tons of biogenic silica with limited economic value (<500 VND kg^{-1}). Rice husk is a unique natural composite containing amorphous SiO_2 (15–22%) with nanoscale particle sizes of 10–50 nm,[11] high surface area (100–200 m^2 g^{-1}),[12] and lignocellulosic carbon (38–42%),[13] with intimate SiO_2/C contact at the nanoscale.[14,15] These intrinsic features make rice husk an attractive precursor for SiC synthesis, offering advantages in cost (200 VND kg^{-1} for rice husk versus ~15 000 VND kg^{-1} for conventional raw materials), reduced reliance on external carbon sources, and mitigation of environmental pollution associated with open-air husk burning.

Numerous studies have therefore explored the synthesis of SiC from rice husk via carbothermal reduction, as summarized in Table 1. However, the fundamental limitation of the solid-state reaction ($SiO_2(s) + 3C(s) \rightarrow SiC(s) + 2CO(g)$) lies in sluggish solid-state diffusion kinetics, which typically necessitate temperatures above 1500 °C to overcome activation barriers despite favorable thermodynamics.[16]

Table 1. Overview of representative studies on SiC synthesis from rice husk.

Author / Year	Temperature (°C)	SiC (wt%)	Catalyst	Limitation	Ref.
Pereira et al., 2020	1600-1800	40-60	-	High temperature	17
Tran et al., 2024	1375	65 (whiskers)	-	Low yield	18
Kieu et al., 2024	1200	20,4	Na_2SiO_3	Temperature not optimized	19
Kieu et al., 2024	1200	18,3	Na_2SiO_3	Low yield	15
Trung et al.,2020	-	85.12		Complex equipment	20

To address this challenge, transition-metal catalysts such as Fe, Ni, and Cu have been introduced to lower the reaction temperature through a Vapor–Liquid–Solid (VLS) mechanism.[21,22] In this mechanism, the formation of the metal–silicon eutectic generates a transient liquid phase that markedly enhances atomic diffusion and accelerates SiC formation. Among these catalysts, Cu exhibits the lowest eutectic temperature, minimal magnetic contamination, and reduced propensity for undesired phase transformations compared with Fe and Ni.[23-25]

Despite these advantages, most Cu-catalyzed studies have primarily focused on varying Cu content, while the systematic influence of calcination temperature in the range of 900–1300 °C at fixed feedstock composition remains insufficiently explored.[25] Moreover, the combined use of silica gel to compensate for SiO_2 deficiency in rice husk and the optimization of post-thermal treatment coupled with purification have received limited attention. Therefore, this study aims to elucidate the effect of calcination temperature on Cu-assisted synthesis of SiC from a rice husk–silica gel mixture. By fixing the feedstock composition and varying the calcination temperature from 900 to 1300 °C, the optimal conditions for phase formation were identified through systematic evaluation of SiC yield, phase composition, and microstructural evolution. The effectiveness of HF purification in enhancing SiC content was also assessed.

2. Experimental method

2.1. Materials

Rice husk (RH), collected from Tay Ninh Province, Vietnam, was used as the primary precursor providing both silica and carbon. The raw rice husk was thoroughly washed with distilled water, dried at 110 °C, and subsequently ground into fine powder. The average particle size of the milled rice husk, determined by laser particle size analysis, was 13.12 μm. The chemical composition of the rice husk is summarized in Table 2.

Silica gel (SG) was synthesized from sodium silicate (Na_2SiO_3) and hydrochloric acid (HCl) following the procedure reported in [26]. The synthesized silica gel was dried, ground, and characterized for particle size and chemical composition. The average particle size of the ground silica gel was 14.93 μm, and its chemical composition is also presented in Table 2. Silica gel was used to compensate for the SiO_2 deficiency of rice husk in the feedstock mixture.

Copper powder (purity >99%, industrial grade) was employed as a catalytic additive to promote SiC formation. Hydrofluoric acid (HF, 50 %wt.) was diluted to 10 wt% and used for post-synthesis purification of the SiC products.

Table 2. Chemical composition of rice husk and silica gel (%wt.).

Material	Si	Na	K	S	Fe	C	N	H	Others
RH	6.96	0.08	0.15	0.07	0.31	45.92	3.12	6.13	35.26
SG	67.20	1.75	0.12	0.06	-	-	-	-	30.87

Sample Preparation and Synthesis

A schematic illustration of the experimental workflow is presented in **Figure 1.**

Feedstock preparation - Rice husk, silica gel, and Cu powder were weighed according to fixed mass ratios. The rice husk/silica gel ratio was maintained at 1:1.4, while the rice husk/Cu ratio was fixed at 1:2. The powders were dry-mixed using a planetary ball mill at a rotational speed of 400 rpm for 2 min to ensure homogeneous dispersion of all components. The mixed powder was then pressed into cylindrical pellets with a diameter of 10 mm and a height of 8 mm under a compaction pressure of 2 MPa.

Thermal treatment - Carbothermal reduction was conducted in a horizontal tube furnace. The pellets were placed in high-purity alumina crucibles (Al_2O_3, 99%) and heated at a constant heating rate of 10 °C min^{-1} under a CO_2 protective atmosphere. The calcination temperatures investigated were 900, 1000, 1100, 1200, and 1300 °C, with a 60-minute holding time at the target temperature. After the carbothermal reaction, the furnace temperature was rapidly decreased to 800 °C, followed by an isothermal holding step for 60 min in ambient air. Finally, the furnace was allowed to cool naturally to room temperature.

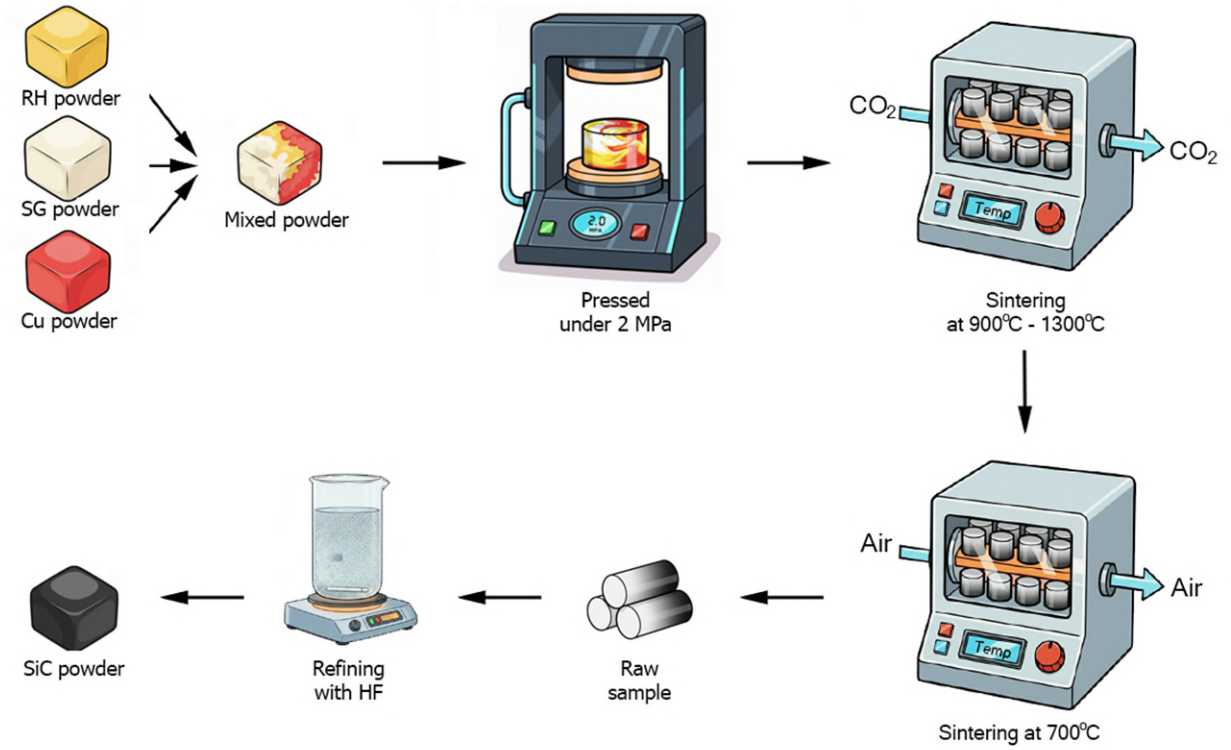


Figure 1. A Diagram of the prototyping process

2.2. Characterization Techniques

Determination of SiC, SiO_2, and free carbon contents - Both as-synthesized and HF-purified samples were analyzed for SiC, SiO_2, and free carbon contents according to ISO 21068–2:2008. Total carbon was determined by oxidation with tin powder in a tube furnace at 1050 °C, converting carbon to CO_2 via combustion. Free carbon was selectively oxidized to CO_2 using a chromic–sulfuric–iodic acid mixture at 130–140 °C. In both cases, the generated CO_2 was absorbed in sodium hydroxide (NaOH) solution. Total carbon and free carbon contents were calculated using Eqs. (1) and (2), respectively. The SiC content was

subsequently calculated from the difference between total carbon and free carbon using Eq. (3). SiO_2 content was determined by dissolution in hydrofluoric acid based on the chemical reactions described in Eqs. (4) and (5).

$$\%C_{total} = 0{,}2729 * (\Delta m/m_{01}) * 100\% \quad (1)$$

$$\%C_{free} = 0{,}2729 * (\Delta m/m_{02}) * 100\% \quad (2)$$

$$\%SiC = 3{,}3383 * (\%C_{total} - \%\%C_{free}) \quad (3)$$

$$SiO_2 + 2KF + 4HF \rightarrow K_2SiF_6 + 2H_2O \quad (4)$$

$$K_2SiF6 + 4NaOH \rightarrow 2KF + 4NaF + SiO_2 + 2H_2O \quad (5)$$

Where $\%C_{total}$ is the total carbon content (%), $\%C_{free}$ is the free carbon content (%), %SiC is the SiC content (%), Δm is the mass increase of the NaOH solution during CO_2 absorption (g), $m_{01}$and m_{02} are the initial masses of the composite samples for total carbon and free carbon determination (g), respectively. The factor 0.2729 converts CO_2 to carbon, while 3.3383 is the stoichiometric conversion factor from carbon to SiC.

X-ray diffraction (XRD) - Phase composition was identified by X-ray diffraction using an EMPYREAN diffractometer (PANalytical) with Cu Kα radiation. Diffraction patterns were recorded over a 2θ range of 15–75° with a step size of 0.02°.

Fourier transform infrared spectroscopy (FTIR) - Chemical bonding and functional groups were analyzed using a Nicolet 6700 FTIR spectrometer (Thermo Scientific) with the KBr pellet method in the wavenumber range of 450–3900 cm^{-1} at a resolution of 1.93 cm^{-1}.

Scanning electron microscopy and energy-dispersive X-ray spectroscopy (SEM/EDX) - Microstructural features and semi-quantitative elemental distributions were examined using a JSM-IT200 scanning electron microscope (JEOL) equipped with an EDX detector. SEM images were acquired at magnifications of ×1000 and ×5000 using an accelerating voltage of 10 kV, a working distance of 11.5 mm, and secondary electron imaging mode.

3. Results & Discussion

3.1. SiC yield before purification and effect of calcination temperature

Figures 2 and 3 present the chemical composition of the as-synthesized products obtained at different calcination temperatures, determined according to ISO 21068-2:2024. As shown in Figure 2, the SiC content in the raw products increases progressively from 22.72% at 900 °C to a maximum of 44.12% at 1300 °C, clearly revealing three distinct kinetic regimes for the carbothermal reduction reaction in the rice husk–silica gel–Cu system.

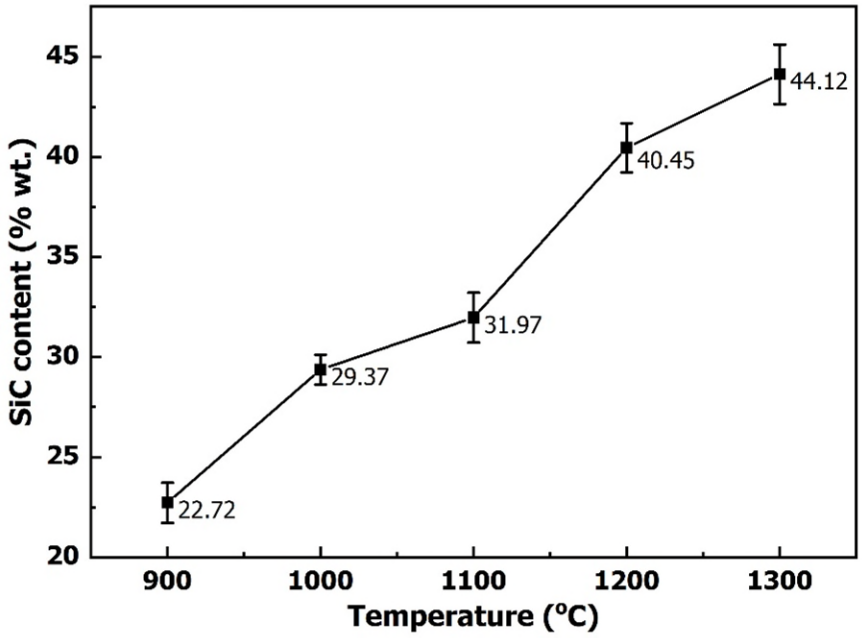


Figure 2. SiC content in products before HF purification

In the first regime (900–1100 °C), SiC formation is limited by the high activation energy of the solid-state reaction, leading predominantly to the formation of amorphous intermediates. The average increase in SiC yield in this temperature range is 4.63% per 100 °C, consistent with diffusion-controlled kinetics (reaction (6)). In the intermediate regime (1100–1200 °C), enhanced atomic mobility significantly accelerates the reaction, resulting in a higher SiC growth rate of 8.48% per 100 °C. In the final regime (1200–1300 °C), the increase in SiC content becomes less pronounced (3.67% per 100 °C), which can be attributed to the establishment of a dynamic equilibrium between SiC formation and reverse oxidation reactions, as described by reaction (7).

The post-calcination thermal treatment at 800 °C in air plays a critical role in increasing the SiC content compared with previous studies.[27] This step selectively oxidizes residual free carbon via reaction (8), thereby increasing the relative fraction of SiC in the composite. A similar effect was reported for rice husk pyrolysis, where a 15% increase in SiC content was achieved after oxidation at 700 °C.[17]

$$SiO_2(r) + 3C(r) \rightarrow SiC(r) + 2CO(k) \quad (6)$$

$$SiC(s) + O_2(g) \rightarrow SiO_2(s) + CO_2(g) \quad (7)$$

$$C + O_2 \rightarrow CO_2 \quad (8)$$

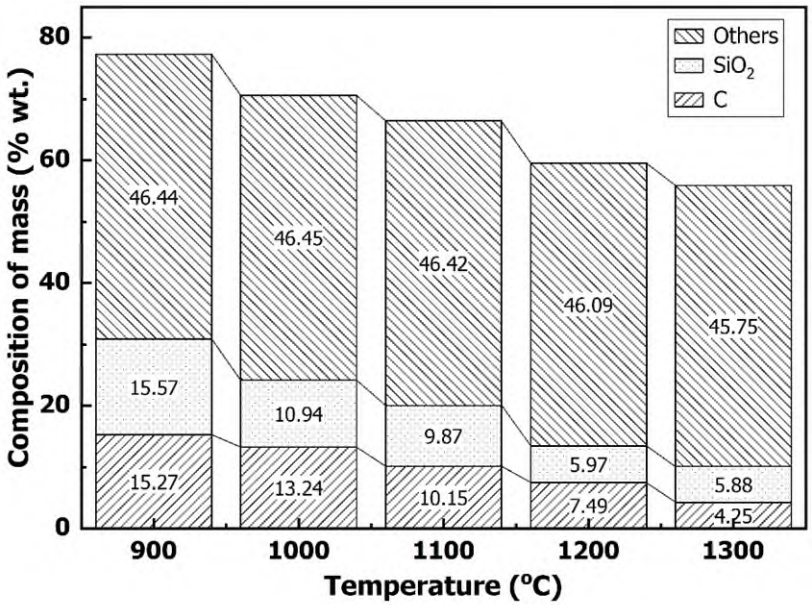


Figure 3. Residual phase composition in products before HF purifacation

Compared with literature data, the SiC yield of 44.12% achieved at 1300 °C is approximately 30% higher than that obtained from rice husk alone under similar conditions,[15] and is comparable to self-propagating high-temperature synthesis from rice husk ash, which typically yields 40–50% SiC.[28,29] Nevertheless, the obtained yield remains lower than the theoretical value (70–80%), which can be attributed to three main limiting factors: (i) deviation of the actual SiO_2/C ratio from the stoichiometric value of 1:3 due to the intrinsic compositions of rice husk (6.96% Si, 45.92% organic carbon) and silica gel (67.20% Si); (ii) the presence of a high fraction of residual phases (~45%) mainly associated with Cu, CuO, and Cu_2O (**Figure 3**); and (iii) the local CO_2-rich atmosphere in the tube furnace, which may hinder complete carbothermal reduction at the pellet surface.

The catalytic role of Cu in enhancing reaction kinetics can be rationalized by the well-established Vapor–Liquid–Solid mechanism. Upon heating, molten Cu (T_m = 1085 °C) forms a low-temperature Si–Cu eutectic in the range of 800–1000 °C, generating a transient liquid phase that markedly increases the diffusion coefficients of Si and C relative to solid-state diffusion. This liquid–solid interface facilitates nucleation and growth of SiC at significantly lower temperatures than those required for uncatalyzed reactions.[25]

Figure 3 further shows that the free carbon content decreases sharply from 15.27% at 900 °C to 4.25% at 1300 °C, confirming the progressive consumption of carbon through reactions (6) and (8). Similarly, the residual SiO_2 content decreases from 15.57% to 5.88%, indicating increasing participation of silica in SiC formation at elevated temperatures. In contrast, the fraction of "other" components remains relatively constant (45.75–46.45%), which is mainly attributed to Cu, CuO, and Cu_2O generated through secondary reactions (9) and (10).

$$Cu + O_2 \rightarrow CuO \quad (9)$$

$$2CuO + CO \rightarrow Cu_2O + CO_2 \quad (10)$$

3.2. Phase composition, molecular structure, and microstructure before purification

The FTIR spectra of the as-synthesized samples shown in **Figure 4** provide direct evidence for the formation of silicon carbide during carbothermal reduction. Characteristic Si–C vibration bands appear at approximately 809 cm^{-1}, corresponding to the stretching mode, and at 624 cm^{-1}, associated with the bending mode, for samples calcined at temperatures of 1100 °C and above. The emergence and progressive intensification of these bands with increasing temperature confirm the onset and advancement of SiC formation, in agreement with previous reports on biomass-derived SiC systems.[30,31] The delayed appearance of these bands at lower temperatures suggests that SiC formation is kinetically limited below 1100 °C, requiring sufficient thermal energy to overcome diffusion and reaction barriers. 1100 °C also corresponds to the melting temperature range of Cu. Thereby promoting the SiC creation process.

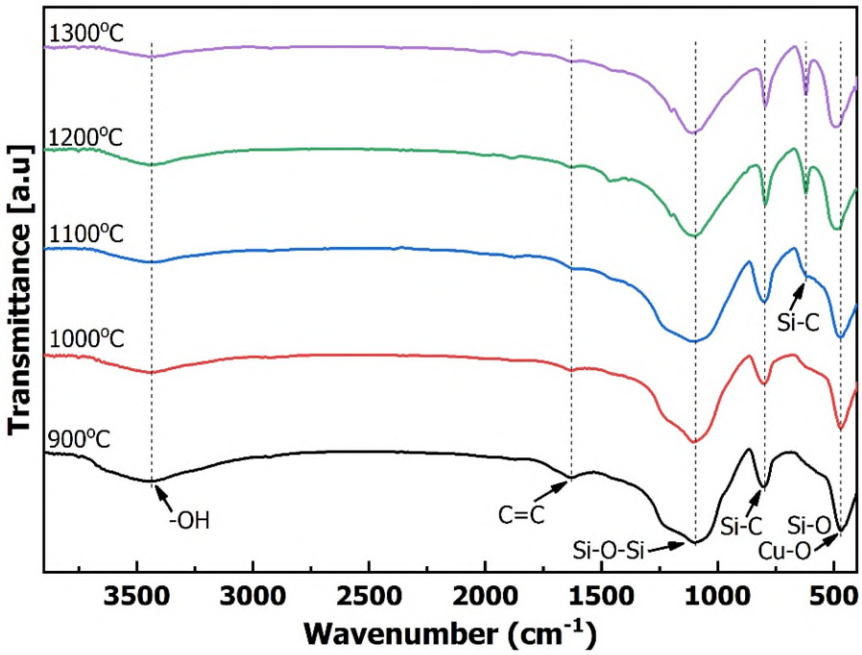


Figure 4. FTIR spectra of products before HF purification

The absorption band at 1633 cm^{-1}, assigned to aromatic C=C stretching vibrations, persists across the entire temperature range but gradually decreases in intensity as the calcination temperature increases from 900 to 1300 °C. This trend indicates partial consumption of free carbon during carbothermal reduction, while also confirming that complete carbon conversion is not achieved even at the highest temperature investigated.[32] The coexistence of residual carbon and SiC is commonly observed in biomass-derived systems due to the heterogeneous distribution of carbon and silica at the microscale and local diffusion limitations during solid-state reactions.

$$SiO_2 \cdot nH_2O \rightarrow SiO_2 + nH_2O \quad (11)$$

A broad absorption band centered at approximately 1110 cm^{-1} corresponds to asymmetric Si–O–Si stretching vibrations, reflecting the presence of residual free SiO_2 that has not fully participated in reaction (6).[33] The persistence of this band across the temperature range suggests incomplete conversion of silica, which can be attributed to the formation of thermodynamically stable crystalline silica phases or physical encapsulation of SiO_2 within carbon-rich regions. The broad –OH stretching band observed at around 3442 cm^{-1} originates from physically adsorbed moisture on the powder surface, which is typical

for porous oxide- and carbide-containing powders exposed to ambient conditions.[34] Additionally, the low-wavenumber band near 480 cm^{-1} can be attributed to overlapping Cu–O lattice vibrations and Si–O bending modes, confirming the presence of copper oxide species, as also indicated by the elemental analysis in **Figure 3**.[35,36] These copper-related phases play a dual role, acting as catalysts for SiC formation while also contributing to impurity phases in the as-synthesized products.

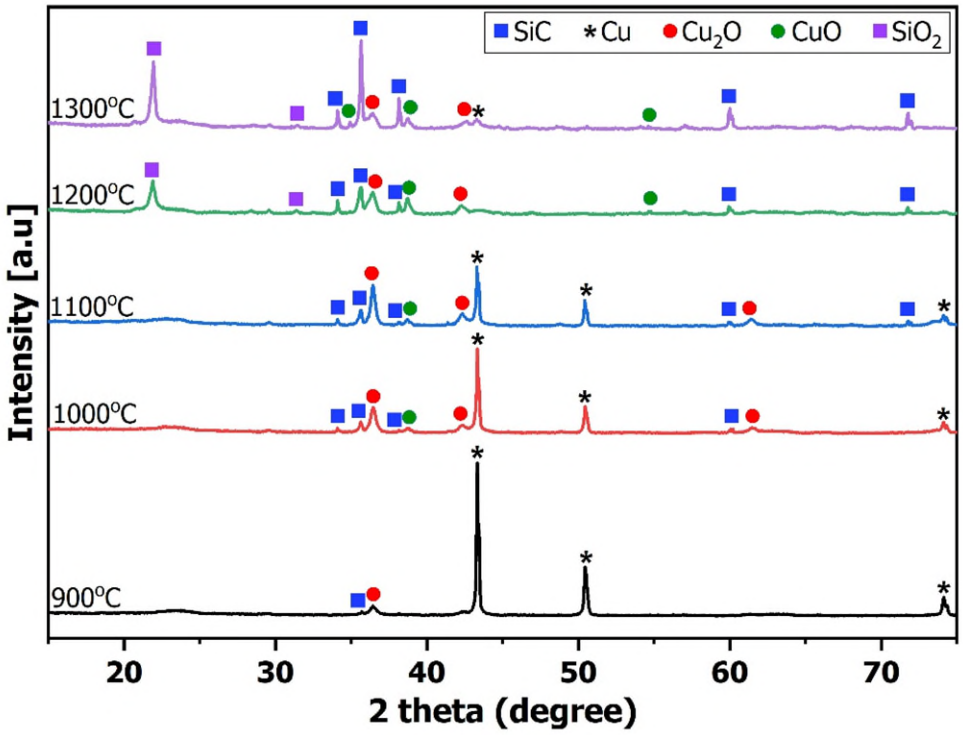


Figure 5. XRD patterns of products before HF purification

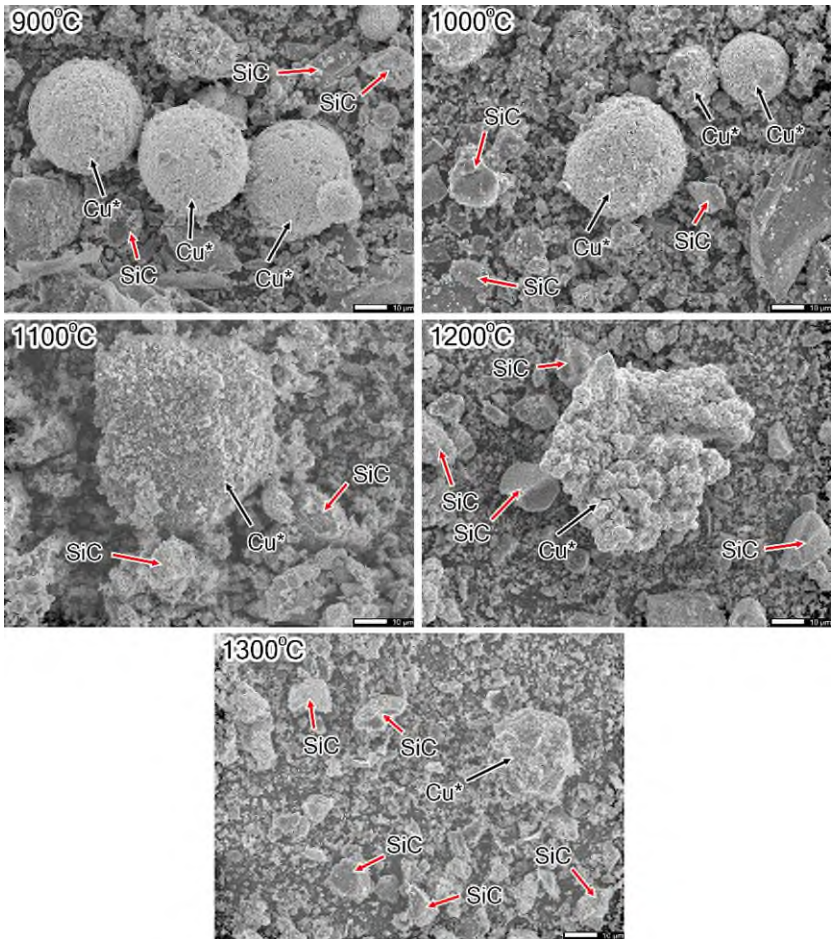
The phase composition inferred from FTIR analysis is further clarified by X-ray diffraction patterns presented in **Figure 5**. The diffraction results clearly demonstrate the formation of cubic 3C-SiC, with characteristic diffractions at 2θ = 35.7° (111), 59.96° (220), and 71.76° (311) (JCPDS 29-1129) [37], alongside hexagonal 4H-SiC, evidenced by peaks at 2θ = 34.1° (100) and 38.1° (102) (JCPDS 29-1127)[38]. The coexistence of cubic and hexagonal polytypes suggests that SiC nucleation occurs under non-equilibrium conditions, where temperature gradients and local compositional variations promote the formation of multiple crystal structures. The gradual narrowing and sharpening of SiC diffraction peaks with increasing calcination temperature indicate enhanced crystallinity and increased crystallite size, as estimated using the Scherrer equation.[39]

Residual silica is primarily detected in the form of cristobalite SiO_2, with characteristic reflections at 2θ = 21.98° (101) and 31.46° (102) (JCPDS 39-1425)[40]. The relative intensity of these peaks becomes more pronounced at 1200 °C, suggesting partial crystallization of initially amorphous silica during thermal treatment. In addition, metallic Cu with a face-centered cubic structure, Cu_2O (cuprite), and CuO (tenorite) are detected (JCPDS 04-0836,[41] 05-0667,[42] and 05-0661,[43] respectively), in agreement with previous studies on Cu-assisted SiC synthesis.[25] The simultaneous presence of Cu, CuO, and Cu_2O at elevated temperatures indicates dynamic redox cycling, where CO partially reduces copper oxides to regenerate metallic Cu, as described by reaction (12). This redox interplay sustains catalytic activity and facilitates SiC formation by enhancing mass transport and lowering the effective reaction temperature.

$$Cu_2O + CO \rightarrow 2Cu + CO_2 \quad (12)$$

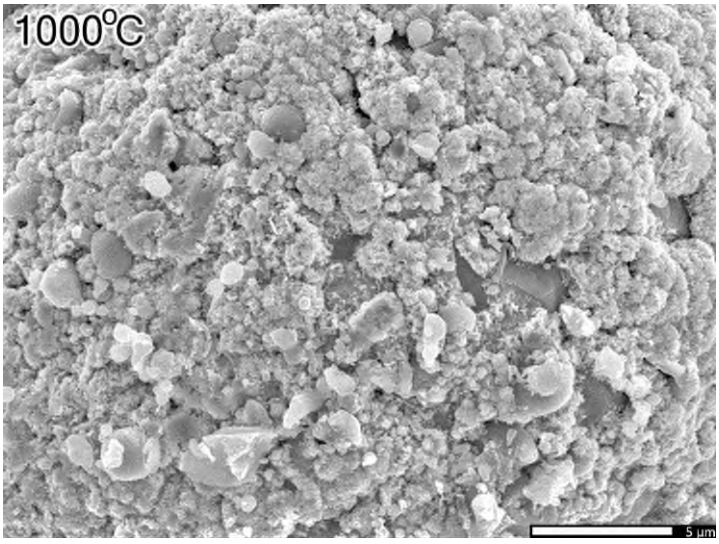
The microstructural changes in the as-synthesized samples are revealed by SEM observations shown in **Figure 6**. At lower calcination temperatures (900–1000 °C), the samples consist of fine, irregular particles with rough surfaces, reflecting the coexistence of SiO_2, carbon, and copper-related phases. As the temperature increases to 1200–1300 °C, SiC particles become more distinguishable and coarser, indicating progressive grain growth and phase development. The rough surface morphology is attributed to the adhesion of residual SiO_2 and CuO phases, which partially coat the SiC particles prior to purification.

Distinct spherical Cu* particles are observed at lower temperatures and gradually evolve into porous or cratered structures at higher temperatures. High-magnification SEM images (**Figure 7**) reveal surface degradation features on Cu* particles, which can be associated with repeated oxidation–reduction cycles between Cu, Cu_2O, and CuO during calcination. These morphological changes are consistent with the participation of copper in catalytic reactions and provide microstructural evidence supporting the Vapor–Liquid–Solid growth mechanism for SiC formation.[44] In this mechanism, transient liquid or semi-liquid Cu–Si phases facilitate Si transport and promote localized SiC nucleation, while continuous redox cycling maintains catalytic efficiency.



275

276 **Figure 6.** SEM images of products before HF purification at magnification 1000×



277

278 **Figure 7.** SEM image of the Cu* surface for the sample calcined at 1000 °C without HF acid
279 treatment (magnification 5000×)

Overall, the combined FTIR, XRD, and SEM results presented in **Figures 4–7** demonstrate that copper effectively enhances the synthesis of silicon carbide from a biomass feedstock via a Vapor–Liquid–Solid-assisted carbothermal reduction pathway. However, this catalytic advantage is accompanied by the formation of residual impurity phases, including SiO_2, Cu, CuO, and Cu_2O, which remain embedded in or adhered to the SiC matrix prior to purification. These observations underscore the necessity of an efficient post-treatment step to selectively remove impurity phases and improve the properties of biomass-derived SiC.

3.3. Properties of SiC after HF purification

Figure 8 shows the SiC content of the products after HF purification, revealing a pronounced increase in SiC concentration across all samples following acid treatment. The maximum SiC content reaches 88.47% at a calcination temperature of 1300 °C, approximately twice that of the corresponding as-synthesized product (44.12%) and exceeding previously reported value for rice husk–derived SiC.[45] This marked increase highlights that a substantial fraction of SiC formed during carbothermal reduction is initially obscured by residual silica and copper-related by-products, rather than reflecting insufficient SiC formation.

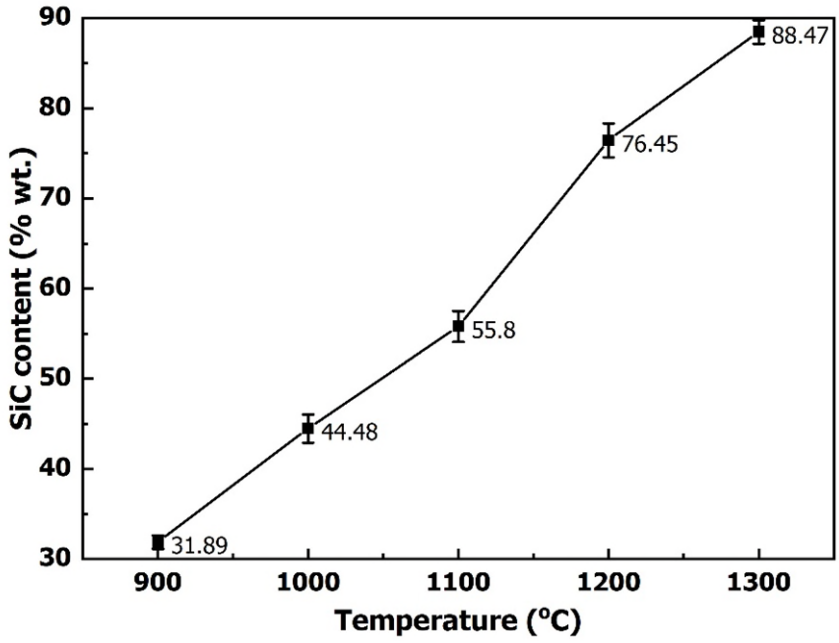


Figure 8. SiC content in products after HF purification

The evolution of SiC yield after purification exhibits two distinct kinetic regimes. In the temperature range of 900–1200 °C, the SiC content increases sharply by approximately

44.56%, corresponding to an average increment of about 14.85% per 100 °C. This rapid enhancement is primarily attributed to the dissolution of residual amorphous or crystalline SiO_2 as well as copper oxides formed during carbothermal reduction. In this regime, HF selectively removes non-SiC phases that coat or embed SiC crystallites, thereby significantly increasing the apparent SiC content without altering the underlying carbide structure. At higher temperatures (1200–1300 °C), the rate of increase becomes less pronounced, indicating a gradual approach toward equilibrium. This behavior is consistent with the diminishing amount of removable impurities and the increasing influence of reverse oxidation reactions, which limit further net gains in SiC content, as discussed in the previous sections.

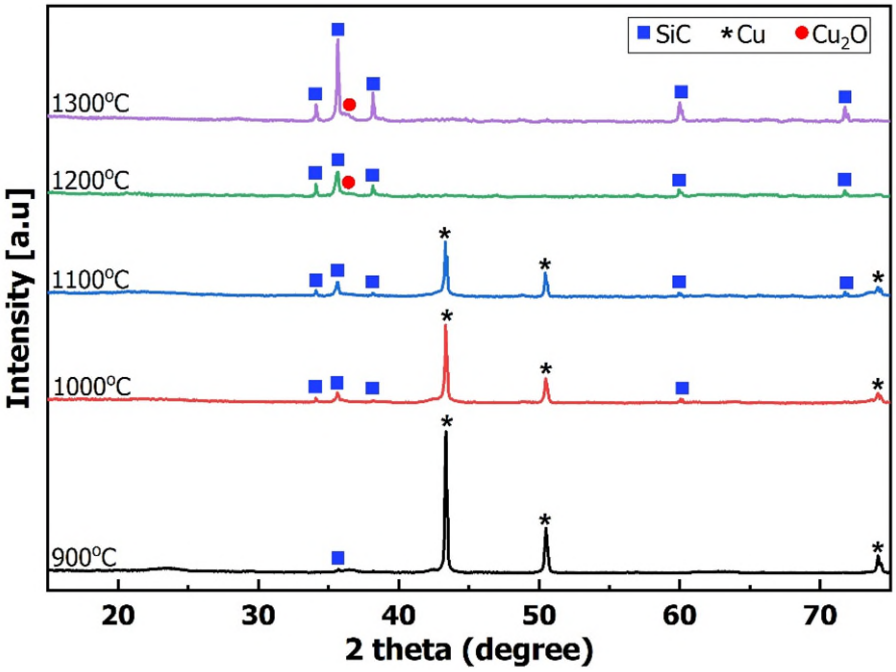


Figure 9. XRD patterns of products after HF purification

The effectiveness and selectivity of HF purification are further corroborated by the XRD patterns shown in **Figure 9**. After treatment, diffraction peaks corresponding to cristobalite SiO_2, CuO (tenorite), and Cu_2O (cuprite) are nearly eliminated. In contrast, diffraction peaks attributed to metallic Cu remain detectable, particularly in samples calcined at 900–1000 °C. This observation is consistent with the known chemical inertness of metallic copper toward HF under ambient conditions. The preferential dissolution of copper oxides follows their basicity, with CuO dissolving more readily than Cu_2O, as described by reactions (13) and (14). Notably, the complete disappearance of SiO_2-related diffraction peaks confirms that HF

purification effectively removes residual silica, a significant obstacle to achieving high-purity SiC from biomass-derived precursors.

$$CuO + 2HF \rightarrow CuF_2 + H_2O \quad (13)$$

$$Cu_2O + 2HF \rightarrow Cu + CuF_2 + H_2O \quad (14)$$

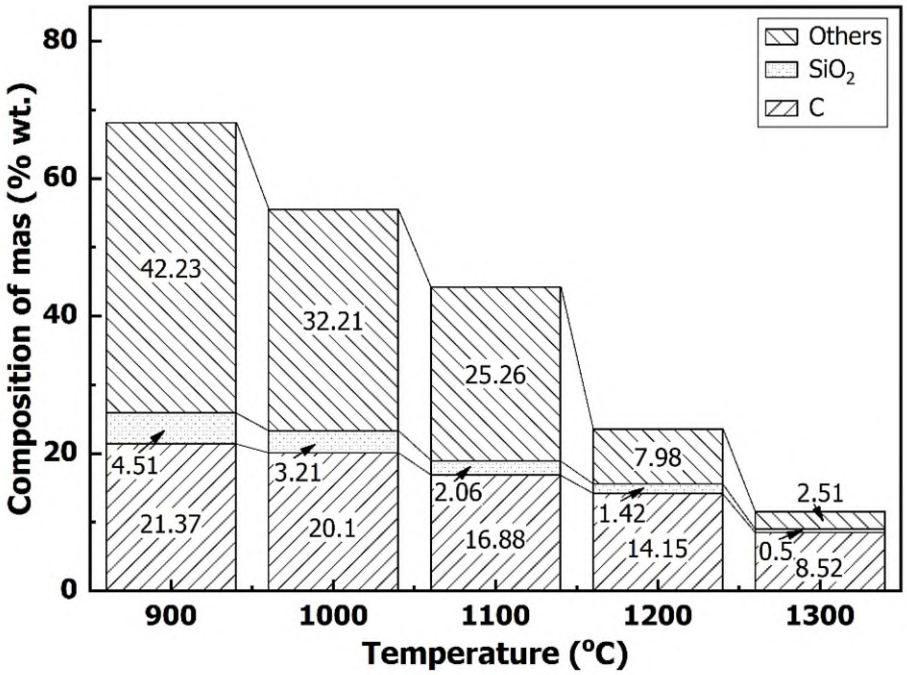


Figure 10. Residual phase composition after HF purification

Quantitative phase analysis after purification, summarized in **Figure 10**, provides information on the change in impurity phases with increasing calcination temperature. The SiO_2 content decreases markedly to 4.51% at 900 °C and 0.50% at 1300 °C, confirming the efficiency of HF in dissolving silica via reaction (15). The persistence of small amounts of silica at higher temperatures may be attributed to its encapsulation within dense SiC aggregates, which can partially hinder acid accessibility. For copper-related impurities, metallic Cu, Cu_2O, and CuO collectively account for 25.26–42.23% of the residual phases at lower calcination temperatures (900–1100 °C). At higher temperatures (1200–1300 °C), however, the residual copper species are dominated by Cu_2O (2.51–7.98%), as metallic Cu is progressively oxidized during thermal treatment and HF preferentially reacts with the more basic CuO before Cu_2O.[46] These results confirm that the relative reactivity toward HF follows the order CuO > Cu_2O > $SiO_2 \gg Cu(0)$, which is consistent with thermodynamic predictions.

$$SiO_2(s) + 4HF(aq) \rightarrow SiF_4(g)\uparrow + 2H_2O(l) \quad (15).$$

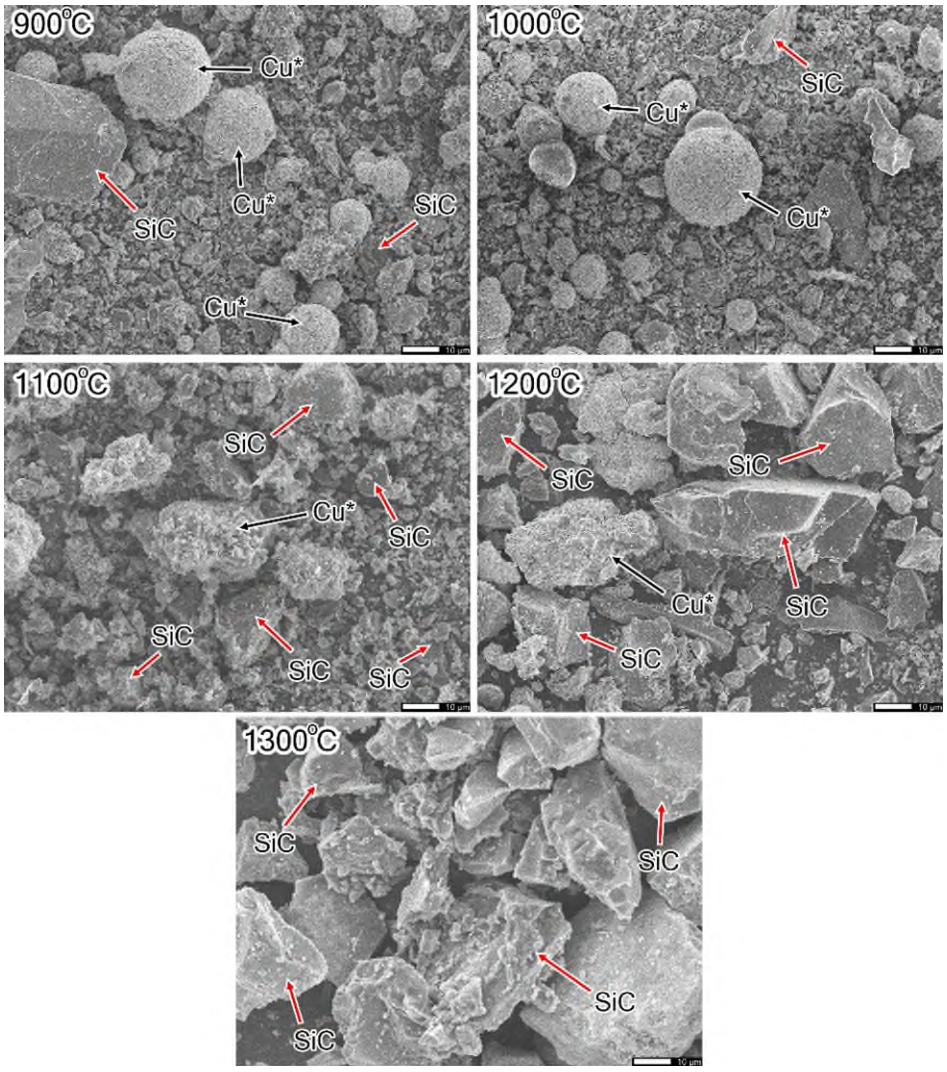


Figure 11. SEM images of products after HF purification (magnification 1000×)

SEM observations after HF treatment (**Figure 11**) provide complementary morphological evidence for the effective removal of impurity phases. Compared with the as-synthesized samples (**Figure 6**), the purified products exhibit sharply defined SiC particles with clean, well-resolved surfaces, indicating that surface-adsorbed silica and copper oxide layers have been successfully removed. The exposure of faceted SiC grains suggests that HF treatment not only removes impurities but also reveals the intrinsic morphology of the carbide phase. At lower calcination temperatures, residual spherical Cu particles remain visible, consistent with the limited chemical interaction between metallic Cu and HF. Notably,

no signs of surface etching or structural degradation of SiC are observed, confirming its chemical stability under the applied purification conditions.

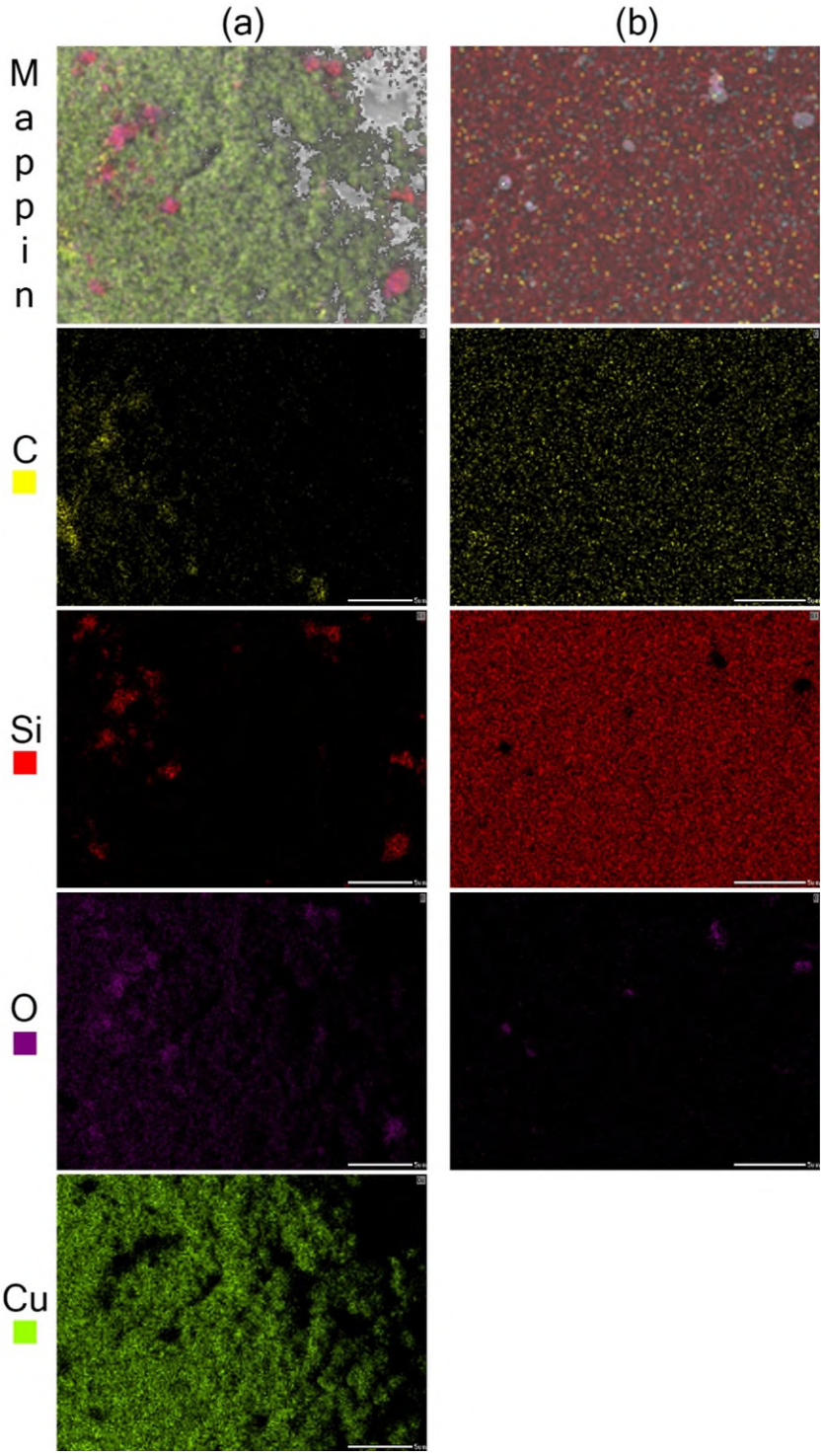


Figure 12. Elemental distribution map of the sample calcined at 1300 °C before (a) and after (b) HF acid treatment

Elemental distribution maps obtained by EDX for samples calcined at 1300 °C, before and after HF purification (**Figure 12**), further alter the compositional evolution induced by acid treatment. A substantial reduction in Cu and O signals is observed after purification, indicating the effective removal of copper oxides and silica. Concurrently, the relative intensities of Si and C increase markedly and become more uniform, confirming that the purified product is predominantly chemically stable SiC. The homogeneous Si–C distribution also suggests that HF purification does not induce elemental segregation or preferential dissolution of the SiC phase.

Collectively, the results presented in **Figures 8–12** demonstrate that HF purification serves as a highly effective and selective post-treatment strategy for enhancing the phase purity of SiC derived from rice husk biomass. By efficiently removing residual silica and copper oxides while preserving the structural and chemical integrity of SiC, this approach significantly improves the apparent yield and quality of the final product. From a sustainability perspective, the ability to achieve high-purity SiC at relatively low synthesis temperatures, combined with an effective purification step, underscores the potential of this biomass-based route as a viable alternative to conventional high-energy industrial processes.

4. Conclusion

A Cu-catalyzed carbothermal reduction route using a rice husk–silica gel feedstock was successfully developed for the synthesis of SiC at 1300 °C. After HF purification, a high SiC content of 88.47% was achieved, representing a twofold improvement over previously reported biomass-based methods (40–75%). This enhancement is attributed to three key factors: (i) formation of a low-temperature Si–Cu eutectic (~800 °C) that overcomes solid-state diffusion limitations via a Vapor–Liquid–Solid mechanism; (ii) a controlled oxidation step at 800 °C that selectively removes free carbon and increases the relative SiC fraction; and (iii) efficient HF purification residual SiO_2 and copper oxide impurities. Compared with the conventional Acheson process (2200 °C, ~9.2 t CO_2 per ton of SiC), the proposed method significantly reduces processing temperature and energy demand while valorizing abundant Vietnamese rice husk resources (~20 million tons per year, <200 VND kg^{-1}). This study demonstrated a viable approach for producing high-quality SiC from agricultural biomass, with the potential to scale to continuous processing and achieve high-purity SiC.

References

1. Thevenot, F. A review on boron carbide, *Key Eng. Mater.*, 1991, **56**, 59-88. https://doi.org/10.4028/www.scientific.net/KEM.56-57.59.
2. Porter, L. M. & Davis, R. F. A critical review of ohmic and rectifying contacts for silicon carbide, *Mater. Sci. Eng. B*, 1995, **34**, 83-105. https://doi.org/10.1016/0921-5107(95)01276-1.
3. Davis, R. F., Palmour, J. & Edmond, J. A review of the status of diamond and silicon carbide devices for high-power, -temperature, and -frequency applications, *Int. Electron Devices Meet. Tech. Dig.*, 1990, 785-788. https://doi.org/10.1109/IEDM.1990.237044.
4. Wang, Y., Dong, S., Li, X., Hong, C. & Zhang, X. Synthesis, properties, and multifarious applications of SiC nanoparticles: A review, *Ceram. Int.*, 2022, **48**, 8882-8913. https://doi.org/10.1016/j.ceramint.2021.12.208.
5. Xue, X., Liang, Z., Zhou, J., Zhang, H., Gu, Q., Zhong, Z. & Xing, W. Tubular SiC membranes in brine purification: Effects of operational parameters towards low energy consumption process, *Sep. Purif. Technol.*, 2025, **366**, 132736. https://doi.org/10.1016/j.seppur.2025.132736.
6. Mühlbauer, A., Keiner, D., Galimova, T. & Breyer, C. Analysis of production routes for silicon carbide using air as carbon source empowering negative emissions, *Mitig. Adapt. Strateg. Glob. Chang.*, 2024, **29**, 4. https://doi.org/10.1007/s11027-023-10100-6.
7. Luo, H., Luo, R. Y., Wang, L. Y., Huang, P., Cui, G. Y. & Song, J. Q. Effects of fabrication processes on the properties of SiC/SiC composites, *Ceram. Int.*, 2021, **47**, 22669-22676. https://doi.org/10.1016/j.ceramint.2021.04.281.
8. Chiew, Y. L. & Cheong, K. Y. A review on the synthesis of SiC from plant-based biomasses, *Mater. Sci. Eng. B*, 2011, **176**, 951-964. https://doi.org/10.1016/j.mseb.2011.05.037.
9. Dong, S., Zhang, X., Hu, P., Zhang, W., Han, J. & Hu, P. Biomass-derived carbon and polypyrrole addition on SiC whiskers for enhancement of electromagnetic wave absorption, *Chem. Eng. J.*, 2019, **359**, 882-893. https://doi.org/10.1016/j.cej.2018.11.101.
10. Guan, L., Xu, X., Song, L., Song, C., Wang, L., Song, B., Gao, Q., Zhang, X., Shen, H., Wang, W., Yuan, H., Min, Z. & Zhang, R. Biomass carbon-derived SiC nanowires for efficient electromagnetic wave absorption, *Mater. Today Nano*, 2025, **32**, 100680. https://doi.org/10.1016/j.mtnano.2025.100680.
11. Mai, N. T., Hoan, L. T., Thuy, H. T. H., Hieu, V. T., Linh, D. T. M. & Vuong, N. T. Nanocomposite coatings based on epoxy resin and nano-SiO2 from rice husk ash: mechanical properties and anti-corrosion to CT3 carbon steel, *Transp. Commun. Sci. J.*,2020, **71**, 1027-1038. https://doi.org/10.47869/tcsj.71.9.2.

12. Nguyen, T. B., Nguyen, N. D., Van Ha, C., Tran, T. T., Ha, K. L. & Nguyen, M. T. Rice husk, activated carbon; Activated carbon from rice husks: synthesis, characterization, and application to enhanced Cr(III) and Pb(II) adsorption from aqueous solutions, *Hue Univ. J. Sci.: Nat. Sci.*, 2023, **132**, 83-93. https://doi.org/10.26459/hueunijns.v132i1A.6943.
13. Sharma, N., Allardyce, B. J., Rąkhowa, R. & Agrawal, R. Rice straw-derived cellulose: a comparative study of various pre-treatment technologies and its conversion to nanofibres, *Sci. Rep.*, 2023, **13**, 13627. https://doi.org/10.1038/s41598-023-43535-7.
14. Hamidu, I., Afotey, B., Kwakye-Awuah, B. & Anang, D. A. Synthesis of silica and silicon from rice husk feedstock: A review, *Heliyon*, 2025, **11**, 429491. https://doi.org/10.1016/j.heliyon.2025.e42491.
15. Kien, K. D. T., Dieu, H. O., Thien, K. N. H. & Ngoc, M. H. Effect of rice husk morphology on the ability to synthesize silicon carbide by pyrolysis method, *Vietnam J. Sci. Technol.*, 2023, 63, 916-923. https://doi.org/10.15625/2525-2518/18511.
16. Liu, C., Yao, S., Yang, X., Tang, C. & Xing, P. A novel Process for Preparing Ferrosilicon Alloy from Coal Gasification Coarse Slag, *Silicon*, 2026, 1-14. https://doi.org/10.1007/s12633-025-03593-0.
17. Pereira, M., Figueira, D., Girolamo, B. & Vernilli, F. Síntese de carbeto de silício a partir de casca de arroz, *Cerâmica*, 2020, **66**, 256-261. https://doi.org/10.1590/0366-69132020663792892.
18. Hien, T. T. T. & Long, N. S. Crystallization of Rice Husk Produced Silica and Silicon Carbide, *Key Eng. Mater.*, 2024, **1005**, 27-32. https://doi.org/10.4028/p-7uttIa.
19. Do, T. K. K., Nguyen, C. T. & Huynh, N. M. Effect of temperature on the ability to synthesize SiC from rice husks, *Mater. Res. Express*, 2024, **11**, 055510. https://doi.org/10.1088/2053-1591/ad4981.
20. Trung, T. V. & Minh, N. N. Fabrication of Silicon Carbide from Vietnamese Rice Husk Charcoal and Diatomite by Electric Arc Furnaces, *Mater. Sci. Forum*, 2020, **985**, 165-170. https://doi.org/10.4028/www.scientific.net/MSF.985.165.
21. Guo, C., Cheng, L., Ye, F. & Zhang, Q. Effect of temperature on the ability to synthesize SiC from rice husks, *Materials*, 2020, **13**, 5179. https://doi.org/10.1088/2053-1591/ad4981.
22. Wang, H., Zepeda-Ruiz, L. A., Gilmer, G. H. & Upmanyu, M. Atomistics of vapour–liquid–solid nanowire growth, N*at. Commun.*, 2013, **4**, 1956. https://doi.org/10.1038/ncomms2956.
23. Chen, B.-Y., Chi, C.-C., Hsu, W.-K. & Ouyang, H. Synthesis of SiC/SiO_2 core–shell nanowires with good optical properties on Ni/SiO_2/Si substrate via ferrocene pyrolysis at low temperature, *Sci. Rep.*, 2021, **11**, 233. https://doi.org/10.1038/s41598-020-80580-y.

24. Shao, J., Zheng, L., Luo, X., Niu, S., Guan, Y. & Huang, H. Preparation of Al2O3-SiC composite powders in the presence of Fe-catalyst via molten-salt-assisted method, *Process. Appl. Ceram.*, 2025, **19**, 374-379. https://doi.org/10.2298/PAC2504374S.
25. Kien, K. D. T. & Minh, H. N. The impact of copper additive content on the synthesis of SiC from rice husks, *Mater. Res. Express*, 2025, **12**, 025502. https://doi.org/10.1088/2053-1591/adb12d.
26. Le, V. H., Thuc, C. N. H. & Thuc, H. H. Synthesis of silica nanoparticles from Vietnamese rice husk by sol–gel method, *Nanoscale Res. Lett.*, 2013, **8**, 58. https://doi.org/10.1186/1556-276X-8-58.
27. Kien, K. D. T. & Nhi, N. V. U. Effect Of Mg/Cu Additives On The Ability To Synthesize SiC From Rice Husk, *J. Appl. Sci. Eng.*, 2025, **28**, 1717-1726. https://doi.org/10.6180/jase.202508_28(8).0009.
28. Chandrasekhar, S., Satyanarayana, K. G., Pramada, P. N., Raghavan, P. & Gupta, T. N. Review Processing, properties and applications of reactive silica from rice husk—an overview, *J. Mater. Sci.*, 2003, **38**, 3159-3168. https://doi.org/10.1023/A:1025157114800.
29. Huang, F., Han, H., Wang, F., Cai, H. & Qin, X. In-situ synthesis of SiC nanowires on biomass carbon materials derived from cherry stones, *Mater. Res. Bull.*, 2023, **167**, 112402. https://doi.org/10.1016/j.materresbull.2023.112402.
30. Sun, Z., Wang, S., Qiao, X., Li, Y., Zheng, W. & Bai, P. Synthesis and microwave absorbing properties of SiC nanowires, *Appl. Phys. A*, 2018, **124**, 802. https://doi.org/10.1007/s00339-018-2202-4.
31. Galvagno, S., Portofino, S., Casciaro, G., Casu, S., d'Aquino, L., Martino, M., Russo, A. & Bezzi, G. Synthesis of beta silicon carbide powders from biomass gasification residue, *J. Mater. Sci.*, 2007, **42**, 6878-6886. https://doi.org/10.1007/s10853-007-1508-y.
32. Kanjana, N., Maiaugree, W., Tontapha, S., Laokul, P., Chingsungnoen, A., Pimanpang, S., Chaiya, I., Daengsakul, S. & Amornkitbamrung, V. Effect of carbonization temperature on the electrocatalytic property and efficiency of dye-sensitized solar cells derived from corncob and sugarcane leaf agricultural residues, *Biomass Convers. Biorefin.*, 2022, **13**, 1-11. https://doi.org/10.1007/s13399-021-02204-3.
33. Oh, T. & Choi, C. K. Comparison between SiOC Thin Film by plasma enhance chemical vapor deposition and SiO_2 Thin Film by Fourier Transform Infrared Spectroscopy, *J. Korean Phys. Soc.*, 2010, **56**, 1150-1155. https://doi.org/10.3938/jkps.56.1150.
34. Waheed, Y., Iram, S., Ahmad, K., Ashraf, G. & Almarhoon, Z. A comparative study of gallium doping on electrochemical and optical properties of green synthesized FeO–MgO nanoparticles using *Citrus Nobilis*, *J. Appl. Electrochem.*, 2024, **54**, 2769-2779. https://doi.org/10.1007/s10800-024-02147-3.

35. Dehaj, M. S. & Mohiabadi, M. Z. Experimental study of water-based CuO nanofluid flow in heat pipe solar collector, *J. Therm. Anal. Calorim.*,2019, **137**, 2061-2072. https://doi.org/10.1007/s10973-019-08046-6.
36. Andrés Serrano, E. S., del Prado, Á., Martinez-Viviente, F., Mártil, I., Bravo, D. & López, F. Rapid thermal annealing effects on the structural properties and density of defects in SiO_2 and SiN_x:H films deposited by electron cyclotron resonance, *J. Appl. Phys.*,2000, **87**, 1187-1192. https://doi.org/10.1063/1.371996.
37. Li, T., Xu, L., Wang, L., Yang, L. & Qian, Y. Synthesis and characterization of 3C and 2H-SiC nanocrystals starting from SiO_2, C_2H_5OH and metallic Mg, *J. Alloys Compd.*, 2009, **484**, 341-346. https://doi.org/10.1016/j.jallcom.2009.04.096.
38. Wu, H., Liu, Z., Xiao, Z., Chen, Y. & Chen, X. Gold Nanoparticle-Decorated Bamboo-Like 4H-SiC Nanowire Field Emitters With Low Turn-on Field and Minimal Current Fluctuations, *IEEE Trans. Electron Devices*, 2025, **72**, 4434-4439. https://doi.org/10.1109/TED.2025.3580694.
39. Holzwarth, U. & Gibson, N. The Scherrer equation versus the 'Debye-Scherrer equation', *Nat. Nanotechnol.*, 2011, **6**, 534-534. https://doi.org/10.1038/nnano.2011.145.
40. Hojamberdiev, M., Eminov, A. & Xu, Y. Utilization of muscovite granite waste in the manufacture of ceramic tiles, *Ceram. Int.*, 2011, **37**, 871-876. https://doi.org/10.1016/j.ceramint.2010.10.032.
41. Jiang, Z., Zhang, Q., Zong, C., Liu, B. J., Ren, B., Xie, Z. & Zheng, L. Cu–Au alloy nanotubes with five-fold twinned structure and their application in surface-enhanced Raman scattering, *J. Mater. Chem.*, 2012, **22**, 18192-18197. https://doi.org/10.1039/C2JM33863G.
42. Miao, Y., Zhang, X., Sui, Y., Hu, E., Qi, J., Wei, F., Meng, Q., He, Y., Sun, Z., Ren, Y. & Zhan, Z. Nanospherical Cu_2O/NiO synthesized by electrochemical dealloying as efficient electrode materials for supercapacitors, *Mater. Lett.*, 2020, **265**, 127300. https://doi.org/10.1016/j.matlet.2020.127300.
43. Liu, X., Li, Z., Zhang, Q., Li, F. & Kong, T. CuO nanowires prepared via a facile solution route and their photocatalytic property, *Mater. Lett.*, 2012, **72**, 49-52. https://doi.org/10.1016/j.matlet.2011.12.077.
44. Talabi, H. K. Mechanical Behaviour of Aluminium Hybrid Composites Reinforced with: Rice Husk Ash-Silicon Carbide-Copper Nanoparticles, *Adv. Technol. Mater.*, 2023, **48**, 1-7. https://doi.org/10.24867/ATM-2023-1-001.
45. Minh, D. Q., Khai, T. V., Minh, H. N., Nhi, N. V. U. & Kien, K. D. T. Effect of composition on the ability to form SiC/SiO_2-C composite from rice husk and silica gel, *J. Ceram. Process. Res.*, 2021, **22**, 246-251. https://doi.org/10.36410/jcpr.2021.22.2.246.

46. Hermawan, A., Zhang, B., Taufik, A., Asakura, Y., Hasegawa, T., Zhu, J., Shi, P. & Yin, S. CuO Nanoparticles/$Ti_3C_2T_x$ MXene Hybrid Nanocomposites for Detection of Toluene Gas, *ACS Appl. Nano Mater.*, 2020, **3**, 4755-4766. https://doi.org/10.1021/acsanm.0c00749.

Acknowledgements

We acknowledge the Ho Chi Minh City University of Technology (HCMUT), VNU-HCM, for supporting this study.

Funding Statement

This research received no external funding.

Author contributions

Kieu Do Trung Kien: conceptualization, performance of experiments, review and editing, project administration. Huynh Ngoc Minh: performance of experiments, analysis and interpretation of data. Nguyen Vu Uyen Nhi: writing – original draft, performance of experiments. Tran Le My Duyen: collection of raw materials, performance of experiments.

Competing interests

The authors declare no competing interests.

Data availability

The data that support the findings of this study are available from the corresponding author upon reasonable request.